International Journal of Advanced Chemistry, 13 (2) (2025) 7-18

International Journal of Advanced Chemistry

Website: www.sciencepubco.com/index.php/IJAC
https://doi.org/10.14419/xmh8yz53
Research paper

Synthesis, Characterization and Biological Evaluation of Novel Macrocyclic Metal Complexes: Insights from Spectroscopic Analysis, Molecular Docking, Antioxidant Studies, and Antimicrobial Screening

Rajrani Gulia [1], Indu Sindhu [1], Anshul Singh [1] *, Neetu Patel [2]

[1] *Department of Chemistry, Baba Mastnath University, Asthal Bohar, Rohtak-124021, India*
[2] *Department of Chemistry, Awadhesh Pratap Singh University, Rewa, M.P. 486003, India*
**Corresponding author E-mail: anshul9008@gmail.com*

Received: June 15, 2025, Accepted: June 15, 2025, Published: June 20, 2025

Abstract

Significant contributions to the development of inorganic chemistry were made by macrocyclic complexes. It has stimulated interest in the study of macrocyclic metal complexes in the design and development of novel antibiotics. In this regard, a series of nine novel macrocyclic complexes of Co(II), Ni(II), and Cu(II) were synthesized by a template approach in a [2:1:2] ratio utilizing o-phenylenediamine and dicarboxylic acid. The newly designed complex's structure has been verified by elemental analysis, Fourier transform infrared, UV-Visible, mass spectrometry, thermogravimetric (TG) analysis, and EPR studies. The Coats-Redfern method was employed for the evaluation of various thermodynamic parameters. Based on the spectral studies distorted octahedral geometry has been proposed around the central metal ion in the synthesized complexes. The synthesized complexes were evaluated against Gram-positive bacteria [*S. aureus*, *B. subtilis*] and Gram-negative [*E. coli, P. aeruginosa*] along with fungal strains [*C. albicans and A. niger*] to assist their antimicrobial potential by agar well diffusion method. Furthermore, the complexes have also been examined for their antioxidant activity utilizing the DPPH assay. Subsequently, molecular docking studies were performed using the Auto Dock Vina programme to assess the biological significance of the synthesized complexes and determine effective binding modes between different ligands and the receptor proteins. The copper macrocyclic complexes demonstrated excellent biocidal action against the selected microbes. Copper acetate exhibited the highest antioxidant potential. The obtained results revealed that the synthesized macrocyclic complexes are potent for making them attractive metal-based antimicrobial and antioxidant prototypes.

Keywords: *Macrocyclic Complexes; Antimicrobial; Antioxidant; Molecular Docking; Template Methodology.*

1. Introduction

Research in physics, biology, and chemical sciences has been emphasized in order to improve the field of macrocyclic chemistry. The significant uses of transition metal macrocyclic complexes in coordination and structural chemistry make them highly fascinating. Metal-coordinated macrocycles have emerged as a key area of study in coordination chemistry [1]. Several synthetic and bioinformatics approaches have been utilized so far to thoroughly investigate the chemical variety of the metal-coordinated macrocycles [2-7]. Comparing synthetic macrocyclic complexes to their open-chain substitutes, they displayed improved thermal stability and resistance to acids and alkalis analogous to natural macrocycles.

Macrocyclic metal complexes have drawn a lot of attention because of their wider variety of uses in herbicidal, anticancer, antiproliferative, antioxidant, anti-inflammatory, and antimicrobial properties. These compounds are also essential to industrial processes. Metal-coordinated macrocycles are well known to have remarkable structural characteristics and enormous potential for use in organic synthesis, thus making them catalysts [8]. The macrocyclic ligands that comprise Oxo (O), Aza (N), Phospha (P), and Sulpha (S) combinations have varying degrees of selectivity for the extraction of metal ions. These factors include the ligand's flexibility, the type of ligand's framework, the size of the cyclic ring, the type and the number of the donor atoms in the cyclic ring, as well as their relative positions within the macrocyclic ligands and the pendant coordinating arms that are attached to the ligand [9-10]. As amide was present in numerous metalloenzymes and the potential for deprotonated amide groups to stabilize higher oxidation states of the metal ions, coordination chemistry employing ligands based on amides becomes particularly fascinating. A different coordination environment around a metal ion was enforced by the amide-based macrocyclic ligands. This surrounding offers an excellent opportunity to gently modify the ligand architecture and has an impact on the framework, redox characteristics, and its reactivity [11-15]. The condensation of o-phenylenediamine with different aromatic dicar-

boxylic acids yields a significant class of tetra-amide macrocyclic ligands. Amide macrocyclic complexes have several applications, including homogenous catalysis and electro-phosphorescence devices [16]. Our current investigation was initiated as a result of these observations. Consequently, we describe in the present research the one-pot template approach of synthesis, employing phthalic acid and o-phenylenediamine as a template framework, of the nine tetraamide macrocyclic complexes of the first row transition metal ions, including Co(II), Ni(II), and Cu(II). Utilizing elemental analysis, FT-IR, mass spectroscopy, TG analysis, electronic spectroscopy, molar conductance, and EPR studies, the synthesized complexes were characterized. All the synthesized complexes were screened for their antimicrobial properties against the selected microbial strains. Additionally, the antioxidant properties of each complex were investigated. Furthermore, the results of the antimicrobial assay were verified by molecular docking analysis.

2. Experimental

2.1. Materials

Diamine and dicarboxylic acid, and other metal salts are high-purity solvents that were bought from Sigma-Aldrich and used just as obtained. Solvents used for washing and synthesis purposes were of reagent grade.

2.3. Instrumentation

Using KBr pellets, the Fourier-transform infrared (FT-IR) spectra were recorded in the 400-4000cm^{-1} range using a Perkin-Elmer Spectrum BX II. The molar conductance values (HPG System, G-3001) were computed using a digital conductivity metre. A Bruker A300 was used to record the ESR spectra in the X and Q bands. The thermogravimetric analyzer SDT650 has been used for TGA study in the 50–700°C temperature range at a 10°C/min heating rate. The Cary 5000 spectrophotometer was used to record the UV-Vis-NIR spectrum between 200-1000nm in wavelengths. The SCIEX Triple TOF 5600 mass spectrometer was used to measure the mass spectrum.

2.3. Synthesis of macrocyclic complexes [M($C_{22}H_{24}N_4O_4$)X_2]

The one pot template procedure was utilized in the synthesis of macrocyclic complexes by dissolving 10mmol of o-phenylenediamine in 50mL methanolic solution with the divalent metal salts (chloride, acetate or nitrate) of around 5mmol in 20mL of methanolic solution in the ratio of 2:1, this reaction mixture was refluxed for around 1hr leading to the formation of metal amine adduct. Due to the coordination between the metal ion and amine, the slight color variation signifies that the reaction was in progress. Furthermore, Phthalic acid (10mmol) was added to this heated mixture and refluxed for 7-8hr. This mixture was left to cool overnight at room temperature, and the colored precipitates that formed at the bottom of the flask served as a sign that the reaction had ended and the complex had been cyclized. The same procedure has been repeated for synthesizing all the macrocyclic complexes. The products were then isolated, and the precipitates were thoroughly solvent-washed and vacuum-dried. The complexes were soluble in acetone, methanol, isopropyl alcohol, DMF, and DMSO (Scheme 1).

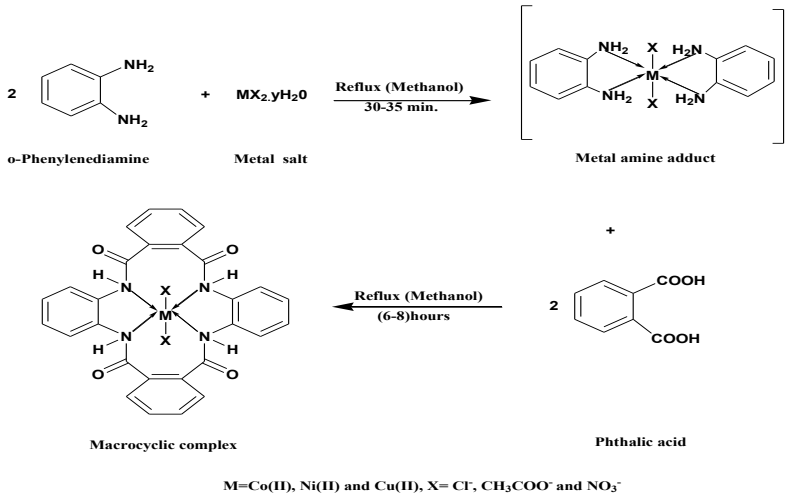

Scheme. 1: Synthetic Scheme for Macrocyclic Complexes [M($C_{28}H_{20}N_4O_4$)X_2].

2.4. Antibacterial activity

The *in vitro* antibacterial activity of each synthesized macrocyclic complex has been assessed. *Staphylococcus aureus* (MTCC 6538), *Bacillus subtilis* (MTCC 6633), whereas [*Escherichia coli* (MTCC 8739), *Pseudomonas aeruginosa* (MTCC 9027)] were chosen as Gram-positive bacteria and Gram-negative bacterial species, respectively for the antibacterial activity assay. Using the Agar well plate diffusion method, the antibacterial activity of macrocyclic complexes has been investigated [17]. For this, 11.5g of Muller Hinton powder was dissolved in 300mL of water, and it was then sterilized by autoclaving it at 121°C for 20minutes. The pH of the medium was kept near 7.4. After cooling, approximately 30mL of the medium was aseptically put into the sterilized petri dishes (100mm x 15mm). After the complexes were dissolved in DMSO, stock solutions were created, and 50µL of each was used in each well. These stock solutions had concentrations of 2.5mg/mL, 5.0mg/mL, and 7.5mg/mL [18]. Agar plates were made in order to cultivate the selected antibacterial strains. After that, the petri plates with the inserted bacteria were incubated at 37°C for around 24 hours. The bacterial potential of all the synthesized complexes was assessed and compared to that of the standard drug Streptomycin [19].

2.5. Antifungal activity

The newly synthesized metal macrocyclic complexes were screened to evaluate their antifungal effectiveness against the fungal strains [*C. albicans* and *A. niger*] using the agar well plate diffusion technique. By combining 19.5g of Sabouraud dextrose agar powder with 300mL of water and sterilizing the mixture at 121°C for 20minutes, an agar medium was obtained. The medium was maintained at a particular pH of 7.2. On the sterile 100mm × 15mm Petri plates, around 30mL of the medium was properly placed after cooling. A sterile brush was used to uniformly distribute the selected fungal strains throughout the plates. Then, a sterile well borer was used to create wells 6mm in diameter with 50µL of macrocyclic complexes at concentrations of 2.5mg/mL, 5.0mg/mL, and 7.5mg/mL. To promote the growth of fungus, the Petri plates' fungal cultures were incubated at 28°C for 48hr. Using a ruler, the average inhibition zone diameter at 6mm wells was measured after incubation, and the calculation was then done to the nearest 0.5mm resolution. The mean and standard deviations of all complexes were computed using the triplicate experiments with DMSO as the solvent. These complexes have been compared to standard medication, Itraconazole [20].

2.6. Antioxidant activity

The DPPH (2,2-diphenyl-1-picrylhydrazyl) test was implemented to assess the complex's ability to scavenge free radicals, and the results were then compared against those of the standard [21].

2.7. DPPH assay

The ability of macrocyclic complexes to neutralize free radicals was evaluated using the DPPH test. The complexes were prepared in concentrations of 3, 6, 9, 12, 15, and 18µg/mL. Ascorbic acid (standard) was diluted with ethanol to a volume of 3mL, and 1mL of an ethanolic DPPH solution (2,2-diphenyl-1-picrylhydrazyl) containing 0.1 mM was added to the complexes. These complexes were incubated at 30°C in the dark for approximately 30minutes. At 517nm, the decrease in DPPH absorbance brought on by regular antioxidant addition, in contrast to the control complex, was evaluated. As a reference, ascorbic acid (10mg/mL DMSO) was used [22, 23]. When DPPH, a free radical solution with a purplish red tone, is scavenged, its colour transforms to yellow. Antioxidant and DPPH solution interact, which causes absorbance to decrease as DPPH is further reduced to DPPH-H. The ability of the synthesized complexes to scavenge DPPH free radicals, at different concentrations and in the standard solution, was tested using their radical scavenging capability (%), which was estimated using below formula:-

$$\text{Radical scavenging capability (\%)} = \frac{\text{Abs. control - Abs. sample}}{\text{Abs. control}} \times 100$$

Where Abs control is the absorbance of DPPH radical and Ethanol; Abs sample is the absorbance of the DPPH radical and macrocyclic complex.

2.8. Molecular docking analysis

In order to confirm the results of antimicrobial activity of the synthesized metal macrocyclic complexes, molecular docking studies were conducted with different bacterial [*S. aureus* (PDB-2DHN), *B. subtilis* (PDB-5H67); *E. coli* (PDB-3T88), *P. aeruginosa* (PDB-2W7Q)] and fungal strains [*C. albicans* (PDB-3DRA), *A. niger* (PDB-6IGY)]. The crystal structure of receptor proteins was downloaded from the RCSB protein data bank, and in AutoDock programme, water molecules were deleted, polar hydrogens were added, Kollmann charges were inserted, and saved receptor protein in pdbqt format. The structure of the synthesized complexes was converted into PDB format with the help of Open Babel software. The grid box was generated, and the program used for docking was AutoDockVina, and the observed structures were envisioned in Biovia Discovery Studio Visualizer [24-26].

3. Results and discussion

3.1. Chemistry

The bioactive macrocyclic tetraaza complexes have been synthesized utilizing template condensation techniques with o-phenylenediamine and Phthalic acid with the general formula $[M(C_{28}H_{20}N_4O_4)X_2]$, where M=Co, Ni, and Cu; X = Cl, Ac, and NO_3 (Scheme 1). Colored solid complexes of synthesized macrocycles were produced. The complexes were found to be soluble in organic solvents such as DMF, DMSO etc. They are non-electrolytes since conductivity values for 10^{-3}M solution in anhydrous DMF are within range of 15 to 32$ohm^{-1}cm^2mol^{-1}$ [27]. The physical properties and analytical data of the complexes are enlisted in the Table 1.

Table 1: Analytical Data of the Macrocyclic Metal Complexes $[M(C_{28}H_{20}N_4O_4)X_2]$

Compound	Empirical Formula	Mol. Wt.	Color	Yield (%)	Analytical % Found (Calculated) C	H	N	O	M	Cl
PO1	$[Co(C_{28}H_{20}N_4O_4)Cl_2]$	606.32	Light Purple	78	55.47 (56.08)	3.32 (4.14)	9.24 (10.14)	10.56 (10.85)	9.72 (10.14)	11.69 (10.14)
PO2	$[Ni(C_{28}H_{20}N_4O_4)Cl_2]$	606.08	Light Blue	73	55.49 (56.16)	3.33 (4.47)	9.68 (10.18)	10.56 (10.69)	9.68 (10.57)	11.70 (10.14)
PO3	$[Cu(C_{28}H_{20}N_4O_4)Cl_2]$	610.93	Black	74	55.05 (56.11)	3.30 (4.19)	9.17 (10.21)	10.48 (10.88)	10.40 (10.86)	11.61 (10.14)
PO4	$[Co(C_{28}H_{20}N_4O_4)(Ac)_2]$	653.5	Light Red	69	58.81 (59.36)	4.01 (5.44)	8.57 (9.12)	19.59 (20.14)	9.02 (10.14)	–
PO5	$[Ni(C_{28}H_{20}N_4O_4)(Ac)_2]$	653.26	Black	77	58.83 (59.11)	4.01 (5.25)	8.58 (9.18)	19.59 (20.59)	8.98 (9.19)	–
PO6	$[Cu(C_{28}H_{20}N_4O_4)(Ac)_2]$	658.12	Green	79	58.40 (59.15)	3.98 (4.16)	8.51 (9.18)	19.45 (20.64)	9.66 (10.58)	–
PO7	$[Co(C_{28}H_{20}N_4O_4)(NO_3)_2]$	659.43	Purple	83	51.00	3.06	12.74	24.26	8.94	

PO8	$[Ni(C_{28}H_{20}N_4O_4)(NO_3)_2]$	659.19	Light purple	68	(45.16) 51.02 (52.18)	(4.45) 3.06 (4.17)	(15.18) 12.75 (13.16)	(25.89) 24.27 (25.84)	(9.57) 8.90 (9.18)	–
PO9	$[Cu(C_{28}H_{20}N_4O_4)(NO_3)_2]$	664.04	Violet	78	50.64 (51.35)	3.04 (4.43)	12.66 (13.12)	24.09 (24.83)	9.57 (9.78)	–

3.2. Infrared spectra

The FT-IR (infrared) spectra of the complexes of dicarboxylic acid and diamines have been obtained and examined for comparison. The lack of free amino acid -NH_2 group in amino acids and -OH groups in carboxylic acid spectrum supports the formation of the macrocyclic complexes (Fig. 1). The absorption band, which corresponds to NH stretching vibration, was visible in the spectra around 3252-3280cm^{-1} [28]. The carbonyl group was represented by a strong absorption band at 1613-1630cm^{-1} and a medium intensity band at 1555-1581cm^{-1}, confirming the cyclization of the product [29]. The phenyl ring absorptions are close to 1400-1419cm^{-1} and 1370-1398cm^{-1}, which are assigned to vasy C_6H_5 and v_{sym} C_6H_5, respectively [30]. The complexes (N-H) amide groups have been recognized through the bands in the 1250-1277cm^{-1} range. Within a range of 1000-1340cm^{-1}, the C-N stretching [31] was observed. Peaks around 412-480cm^{-1} are obtained due to the (M–N) vibration signifying coordination of metal with nitrogen [32]. All of the acetate macrocyclic compounds exhibited bands in the 1412-1537cm^{-1} range [33], and all the nitrate complexes displayed vibration around 1350-1390cm^{-1}, suggesting that the nitrate groups were coordinated to the central metal ion in a unidentate manner [34].

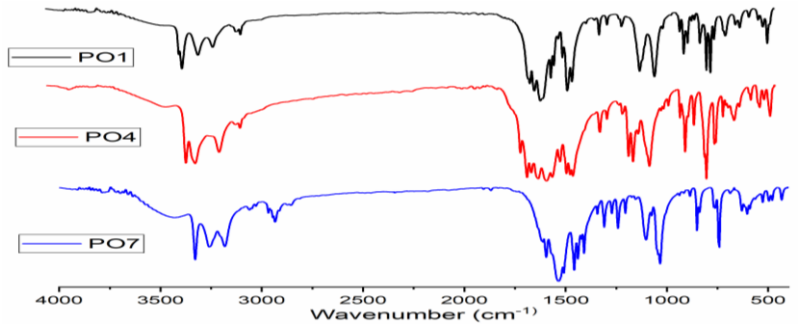

Fig. 1: Infrared Spectra of Macrocyclic Complexes.

3.3. Mass spectra

Mass spectrometry has been utilized to obtain information about the complexes' monomeric or polymeric nature. The proposed molecular formula of the synthesized macrocyclic complexes $[M(C_{28}H_{20}N_4O_4)X_2]$ was confirmed by mass spectroscopy. A molecular ion peak, which was obtained at 614.4833 m/z, corresponds to the chemical formula $[M+Li]^+$ was visible in the copper chloride complex $[Cu(C_{28}H_{20}N_4O_4)Cl_2$. Nickel acetate complex $[Ni(C_{28}H_{20}N_4O_4)(Ac)_2]$ molecular ion peak displayed at m/z 663.4542; due to $[M+2He+H]^+$ for the synthesized macrocyclic complex.

In case of copper nitrate complex $[Cu(C_{28}H_{20}N_4O_4)(NO_3)_2]$, the molecular ion peak occurs at m/z 667.2955 due to $[M+3H]^+$ for the prepared complex in Fig. S1. The monomeric character of the complexes was well supported by the data.

3.4. Thermogravimetric analysis

The thermal properties of the synthesized complexes have been observed. TG curve for the given complex was illustrated in Fig. 2. High thermal stability was seen in the cobalt chloride complex $[Co(C_{28}H_{20}N_4O_4)Cl_2]$, demonstrating the absence of coordinated water molecules in the complex sphere. On the TG curve, the complete breakdown of the copper complex may be seen in 3 stages. The initial 40% weight loss was found between 120-330. The compound loses 23% of its weight between 330 and 425 °C. A 3% weight loss was seen as a result of the third breakdown, which occurred between 455-700. The nickel acetate complex $[Ni(C_{28}H_{20}N_4O_4)(Ac)_2]$ thermogravimetric curve revealed four steps of heat breakdown. According to the TG curve, the initial 52% weight loss was seen throughout a temperature range of 230 to 335 °C. The second breakdown at 340-375°C revealed a weight reduction of 6%. A third 16% weight loss was found in the temperature range 385-430°C and the last breakdown in the range of 425- 800 °C, with 13% weight loss. The thermogram curve of the macrocyclic cobalt nitrate complex $[Co(C_{28}H_{20}N_4O_4)(NO_3)_2]$ showed a three-step breakdown. Weight loss was not seen before 170 °C, confirming that this substance is thermally stable up to 170 °C. The initial 28% weight loss was seen between 170-310°C. When the temperature was between 310-380°C, the second 22% weight loss occurred. A third weight loss of almost 2% occurred between 380-510. The outcomes demonstrate that neither water molecule coordination nor crystallization can be seen [35].

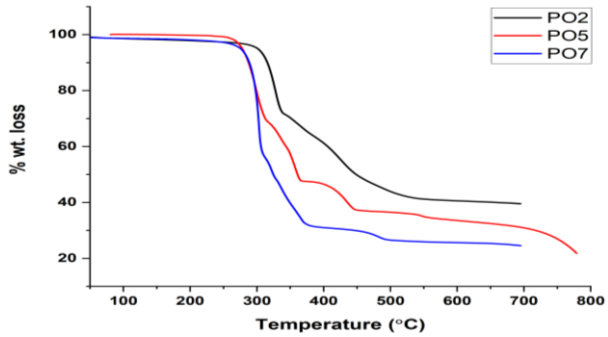

Fig. 2: Thermogravimetric Analysis of Macrocyclic Complexes.

3.5. Kinetic and thermodynamic parameters calculations

Various thermodynamic parameters were calculated using the Coats-Redfern method [36-38] of thermal analysis (Table 2 & Fig. S2) shows that metal complexes show 1st order kinetics as graph plotted Ln(-ln(1-α)/ T^2] v/s 1000/T.

Table 2: Thermodynamic Parameters for the Metal Complexes

Comp.	Temp.	E_a (KJ/mol)	A (s^{-1})	ΔH (KJ/mol)	ΔS (KJ/mol/K)	ΔG (KJ/mol)	R^2
PO2	280ºC	9.76	0.298	5.16	-0.259	148.38	1
	349ºC	9.73	0.260	4.55	-0.261	166.89	0.981
	381ºC	9.96	0.241	4.52	-0.262	175.86	0.978
	616ºC	9.85	0.242	2.45	-0.265	238.03	0.978
PO5	230ºC	8.81	0.293	4.62	-0.259	134.89	0.976
	340ºC	8.72	0.236	3.62	-0.262	164.22	0.988
	385ºC	8.79	0.231	3.31	-0.263	176.36	0.976
	425ºC	8.77	0.225	2.96	-0.263	186.53	0.972
PO7	170ºC	8.72	0.293	5.04	-0.257	130.40	0.975
	310ºC	8.71	0.274	3.86	-0.260	168.84	0.975
	380ºC	8.72	0.275	3.29	-0.261	188.74	0.975

3.6. Electron spin resonance studies

At room temperature, the spectra of the copper tetra aza macrocyclic complex were captured on the X-Band (frequency 8.75–9.65GHz) (Fig. 3). A 3000G magnetic field with a field center of 336.791mT was selected for the analysis. The sweep lasts for four minutes. At room temperature, the spectra of the copper chloride macrocyclic complex $[Cu(C_{28}H_{20}N_4O_4)Cl_2]$ showed an anisotropic signal, and the complex showed a small hyperfine splitting; the values of $g_{\|}$ and $g_{\perp}$ were determined to be 2.08 and 2.016, respectively.

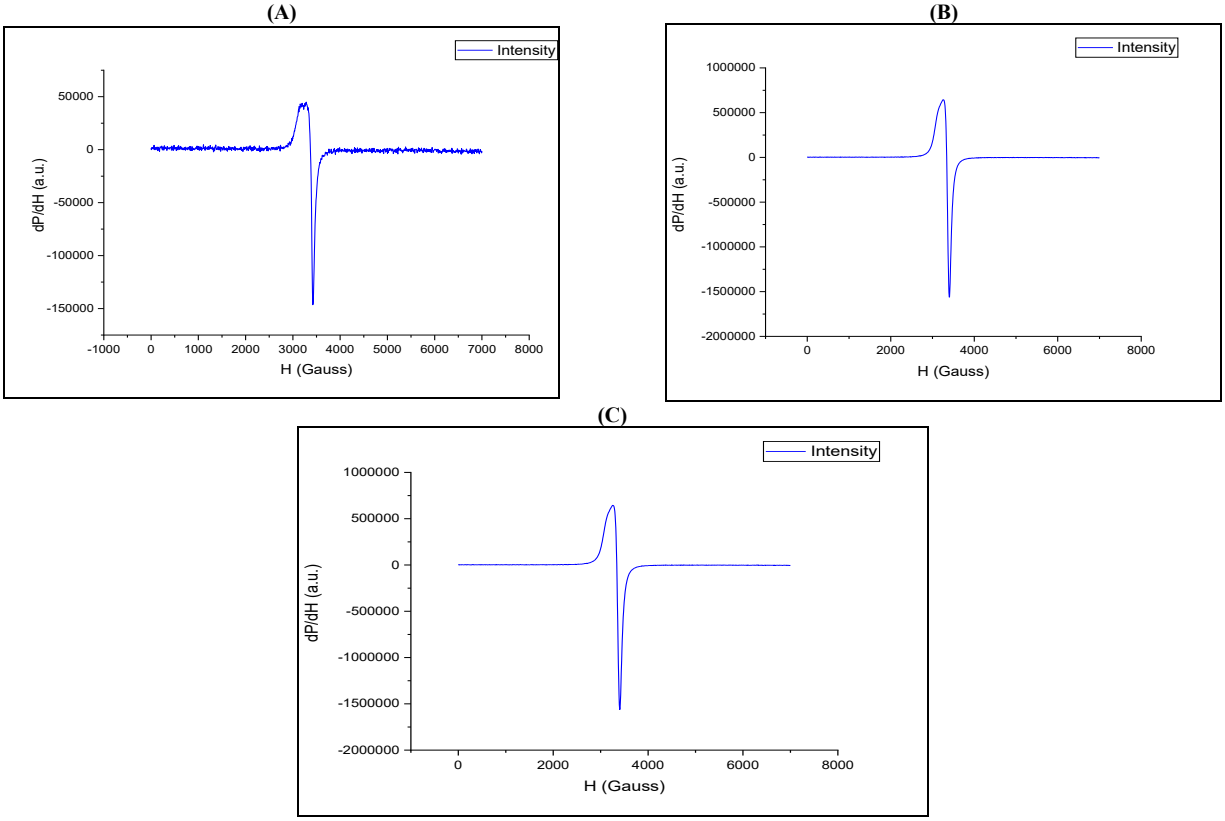

Fig. 3: EPR Spectra of Copper Macrocyclic Complexes of (A) PO3 (B) PO6 and (C) PO9.

The values of g_{iso} for the copper acetate $[Cu(C_{28}H_{20}N_4O_4)(Ac)_2]$ and copper nitrate $[Cu(C_{28}H_{20}N_4O_4)(NO_3)_2]$ complexes have been determined to be 2.18 and 2.016, respectively. At room temperature, these spectra have an isotropic character. The observations revealed the Cu(II) macrocyclic complexes' octahedral shape [39].

3.7. Electronic spectra

The electronic spectra of the synthesized macrocyclic complexes were recorded in DMSO over the range of 200-1000nm. The electronic spectra of metal macrocyclic complexes are shown in Fig. 4.

Cobalt macrocyclic complexes: Co(II) complexes have a magnetic moment of 3.6-3.8B.M., which is equivalent to three unpaired electrons, at room temperature. Bands around 230-270nm and 280-330nm represent π→π* and n→π* transitions. Bands in the range of 380-590nm correspond to d-d transitions. The octahedral geometry is in tune with these transitions [40].

Nickel macrocyclic complexes: Ni(II) complex electronic spectra displayed bands for the π→π* and n→π* transitions at 210–260nm and 270–330nm, respectively. The band around 455- 640nm corresponds to the d-d transition. At room temperature, the magnetic moment is in the 2.64-2.83B.M. range. These numbers are similar to those of the defining characteristics of the octahedral geometry [41].

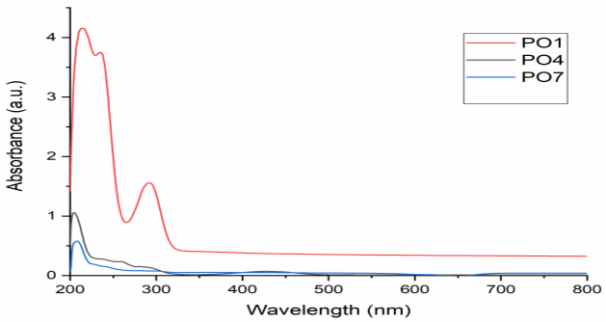

Fig. 4: UV-Vis Spectra of Macrocyclic Complexes.

Copper macrocyclic complexes: Cu(II) complexes magnetic moment has been determined to be 1.6-1.8B.M. The Cu(II) complexes' electronic spectra exhibited bands at ~215- 260nm and ~270-360nm representing π→π* and n→π* transitions. The d-d transitions appeared around 410-580nm. All the complexes' transitions are by the octahedral geometry [42].

3.8. Biological activities

All the synthesized macrocyclic complexes have been studied, and their zones of bacterial growth inhibition have been compared to those of the standard compiled in Table S1. Significant antibacterial action against bacterial species was observed in all of the examined macrocyclic complexes. According to the antibacterial activity data, copper chloride and nitrate macrocyclic complex had the greatest antibacterial efficiency against all types of bacteria except *S. aureus* (Fig. 5,6). Cobalt chloride complex (PO1) exhibited the best zone of inhibition against the bacterium *S. aureus*.

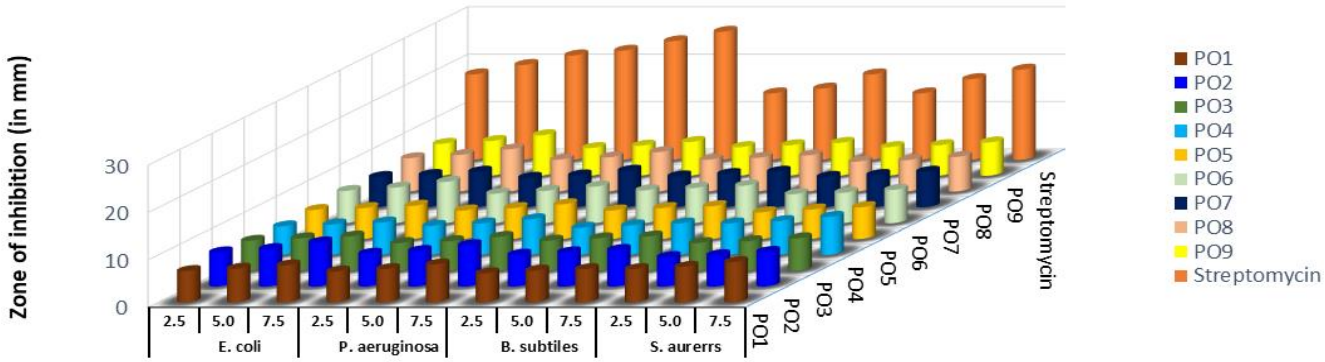

Fig. 5: Zone of Inhibition (Mm) of Synthesized Macrocyclic Metal Complexes $[M(C_{28}H_{20}N_4O_4)X_2]$ Against Bacterial Species at 2.5, 5.0 and 7.5mg/Ml.

A) **B)**

Fig. 6: Zone of Inhibitions of Macrocyclic Complexes A) PO1 Against *S. Aureus* (B) PO2 Against *E. Coli.*

The results of the metal macrocyclic complexes in vitro antifungal examination demonstrated that all the copper complexes (PO3, PO6, and PO9) have the highest antifungal zone of inhibition against *C. albicans* and *A. niger* (Fig. 7,8). These copper complexes demonstrated stronger antifungal potential, displaying their values as prospective broad-spectrum antimicrobial medicines.

These results can be explained using Tweedy's chelation theory, which revealed that the central metal ions' polarity decreases with chelation as the positive charge of the metal ion is shared with the donor groups [43,44]; this further enhances the lipophilic nature of the central metal ion of the macrocyclic complexes. This facilitates fast penetration through the microorganism's cell membranes and lipid layer.

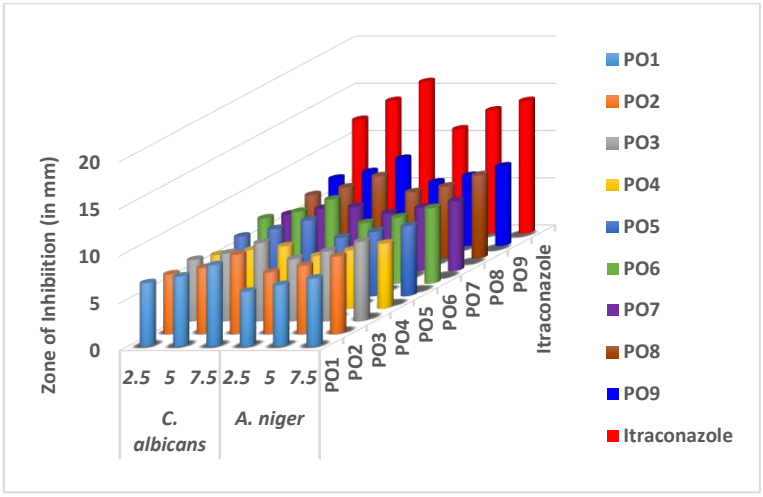

Fig. 7: Zone of Inhibition (Mm) of Synthesized Macrocyclic $[M(C_{22}H_{24}N_4O_4)Cl_2$ Complexes Against Fungal Species at 2.5, 5.0, and 7.5mg/mL.

A) **B)**

Fig. 8: Zone of Inhibitions of Macrocyclic Complexes $[M(C_{28}H_{20}N_4O_4)X_2]$: by (A) PO9 Against *C. Albicans,* (B) PO8 Against *A. Niger*.

3.9. Antioxidant assay

The macrocyclic complexes' DPPH scavenging capabilities were expressed as IC_{50} in Table S2, & Fig. 9, whose concentration was sufficient to produce 50% of their maximum scavenging activity.

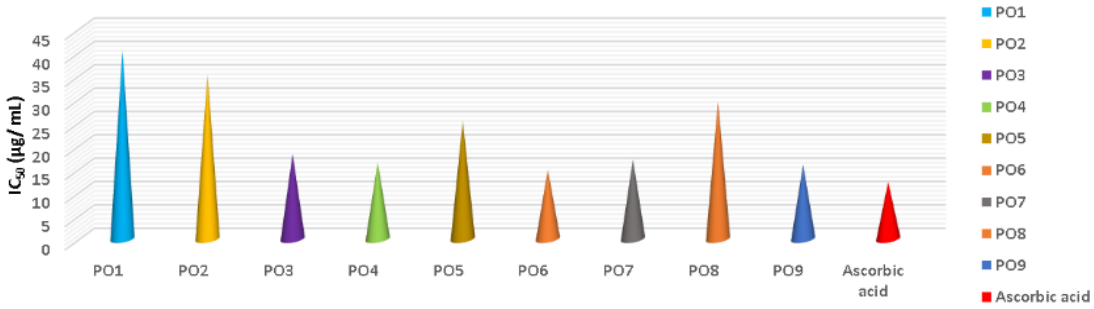

Fig. 9: Antioxidant Activity of Synthesized Macrocyclic Complexes $[M(C_{28}H_{20}N_4O_4)X_2]$.

The results showed that all macrocyclic complexes demonstrated good antioxidant activity, whereas copper acetate (PO6) exhibited close antioxidant action as compared to that of the standard, Ascorbic acid. According to their IC_{50} values against a standard solution - Ascorbic acid, the macrocyclic metal complexes' antioxidant behavior was in the following order: PO6 > PO9 >PO4 > PO7 > PO3 > PO5 > PO8 >PO2 > PO1.

4. Molecular docking

The molecular docking studies were analyzed to examine the molecular properties of the ligand-protein interaction. In this present research, molecular docking was performed for the antimicrobial testing to determine the most likely interaction of the drug and ligand. The energy of the binding affinity describes the favorable binding interaction of the complex with the macromolecule [45-54], and the number of hydrogen bonds represents the stability of the protein-ligand complex, are displayed in Tables 3-5. All macrocyclic metal chloride $[M(C_{28}H_{20}N_4O_4)Cl_2]$ complexes unveil more effectiveness against *E. coli* as revealed by more negative values of the binding energy -12.5Kcal/mol, -13.8Kcal/mol, and -12.2Kcal/mol for PO1, PO2, and PO3 complexes, respectively. Among all synthesized macrocyclic complexes, PO1 complex interacted promisingly with 2DHN receptor protein with the most negative binding affinity -11.5Kcal/mol, exhibiting H-bonding with Val52 amino acid residue, and PO3 displays conventional H-bond interaction with Asp46, Tyr54, and Thr51 residues; while in PO2 complex, no conventional H-bond was observed.

In case 2W7Q protein, the interaction displayed by the PO1 ligand was an H-bond interaction with Gln107, Gln42, and Thr44 amino acid residues. The interaction accompanied by the PO2 ligand is are H-bond with the Gln71, Gln107 residues, and another ligand PO3, exhibits only conventional H-bond interactions with Thr44 and Gln42 amino acid residues. Interaction attributed by PO1 ligand with 3T88 protein was attractive charge interaction with Asp110, Pi-anion interaction with Asp110, Pi-sigma interaction with Ile57, Pi-alkyl interaction with Lys54, Ile57:C, Ile57 D amino residues, while PO2 ligand exhibits conventional H-bond with Gln114, Arg64, Asp110 amino acid residues. However, no H-bond interaction was observed in the PO3 ligand. In another protein 5H67, amino acids Thr27, Ser139, Gln143, and Cys1114 displayed H-bond interaction with PO1 complex and interaction with Ser159 Pi-donor H-bond interaction and conventional H-bond interaction in PO2 ligand. PO3 ligand displays interaction of the three conventional H-bonds with Thr27, Cys1114, and Gln1114 amino acid residues. The PO1 ligand interacts with the 3DRA protein, comprising two H-bonds with Asn30 and Tyr67 residues. However, PO2 complex exhibits two conventional H-bonds with Asn30:ND2 and Tyr67 residues. The interaction in PO3 complexes possesses a H-bond with Tyr297 and Asp294 residues. The 6IGY protein interacts with PO1 ligand through Pi-Pi interaction with Ala152, Val116, and Tyr111 amino acid residues, whereas interaction of PO2 ligand indicates three H-bonds with Tyr150, Glu149, and Tyr111 residues. Interactions exhibited by PO3 are Pi-Pi T-shaped interactions with His262 amino residues.

The molecular docking study reveals that amid all the synthesized macrocyclic complexes, PO1 exhibited the highest binding affinity against *S. aureus,* while PO2 was found to be effective against *E. coli* and *P. aeruginosa* (Fig. 10 & S3-S7). The PO3 complex, however, is less effective against bacterial strains but has a high binding affinity with the 6IGY (*A. niger*) protein.

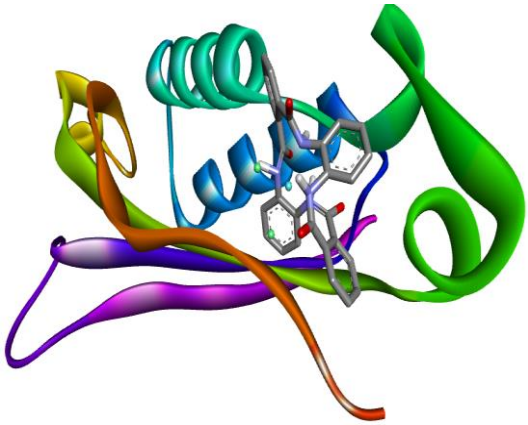

A) 2DHN Interacts with PO1 Ligand

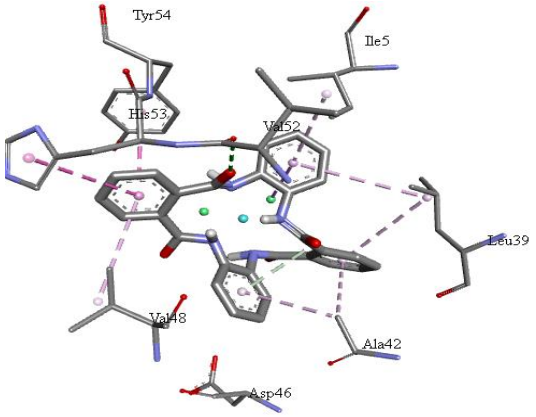

B) 3D Interaction with PO1

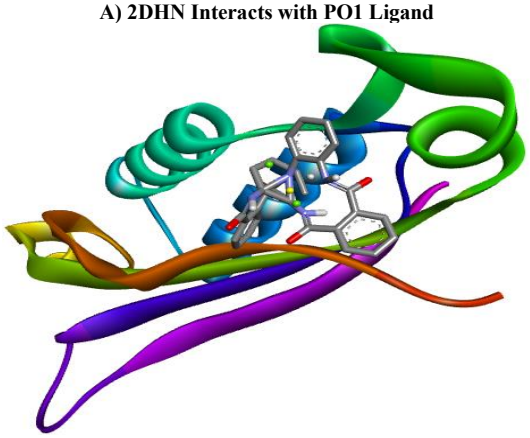

C) Interaction with PO2 Ligand

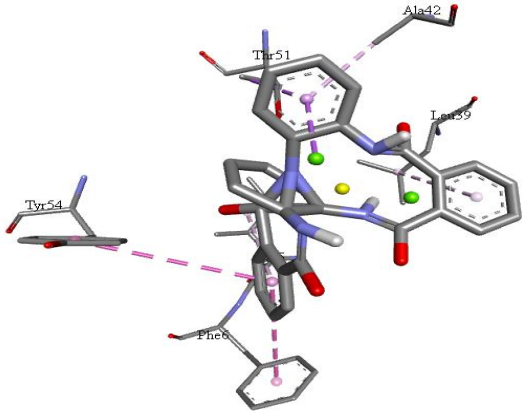

D) 3D Interaction with PO2 Ligand

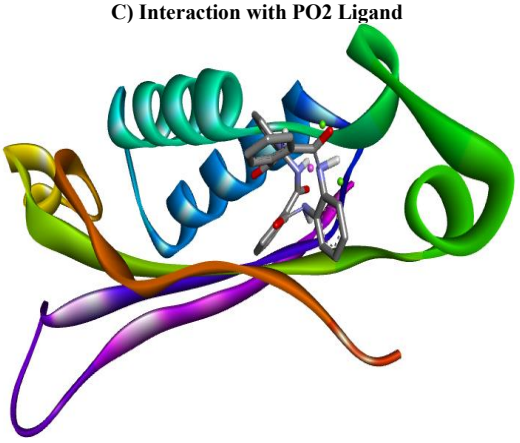

E) Interaction with PO3 ligand

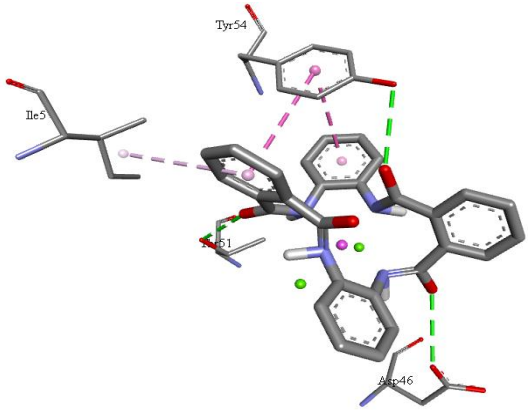

F) 3D interaction with PO3 ligand

Fig. 10: 2DHN Receptor Protein Interaction with Different Metal Complexes (Co in Cyan Color, Cl Ions Are Represented by Green Color, Cu Is in Pink Color, Ni Is in Yellow).

Furthermore, PO4 complex shows more promising effect against 2DHN bacterial strain with -10.1Kcal/mol binding energy with two conventional H-bond interactions with Asp46 and Val52 amino acid residues. In case of 2W7Q protein, three H-bond interactions were observed; two with Gln77, one H-bond with Gln53 residues, with a binding energy of -9.7Kcal/mol. There is no H-bond with 3T88 and 6IGY receptor protein; however, the complex possesses the binding energy of -9.2Kcal/mol and -9.5Kcal/mol, respectively. The 5H67 protein interacts with PO3 complex with a binding energy of -8.4Kcal/mol and exhibits four H-bond interactions with Lys145, Glu163, and Ser52 residues. Interaction with 3DRA receptor protein exhibits one H-bond with Glu156 with -8.6Kcal/mol binding energy.
In contrast, PO5 complex exhibits more effectiveness against 3DRA and 6IGY protein with -10.0Kcal/mol binding energy values and no H-bond interaction with 6IGY receptor; however, three H-bond interactions were observed in the case of 3DRA protein as shown in Table 6. On the other hand, in the case of 3T88 and 5H67 receptor protein binding energy observed was -9.6Kcal/mol and -9.2Kcal/mol with no H-bond interaction. Interaction exhibited with 2DHN protein was only one H-bond with -8.6Kcal/mol energy, and 2W7Q exhibits six H-bond interactions with different amino acid residues possessing a binding energy of -9.5Kcal/mol.
Furthermore, the PO6 complex was showing good results with the 3T88 receptor with -12.9Kcal/mol binding energy and two conventional H-bond interactions. Interaction with 3DRA receptor possessed two H-bonds with -11.3Kcal/mol binding energy. In case of 2DHN and 6IGY, there is only one H-bond interaction observed with -9.2Kcal/mol and -10.4Kcal/mol binding energy values. There are two H-bond interactions with 5H67 and -10.7Kcal/mol binding energy. Three hydrogen bonding interactions were observed with the 2W7Q protein, having -9.8Kcal/mol binding energy. The molecular docking study unveils that among all the synthesized complexes PO6 complex exhibits strong efficacy against *B. subtilis,* while the PO4 complex against *S. aureus*. Amongst all three macrocyclic metal acetate complexes, PO5 was found to be the least effective against all the bacterial and fungal strains (Fig. 11 & S8-12).

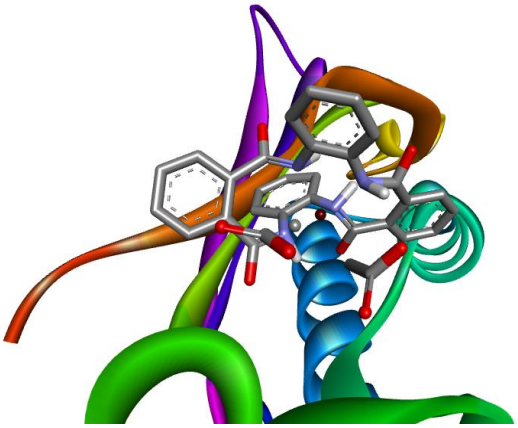

A) Interaction with PO4

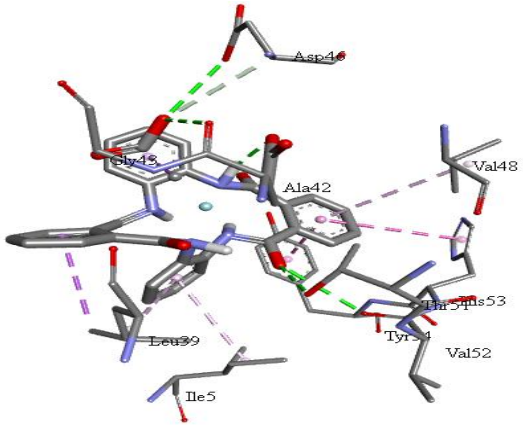

B) 3D Int. with PO4

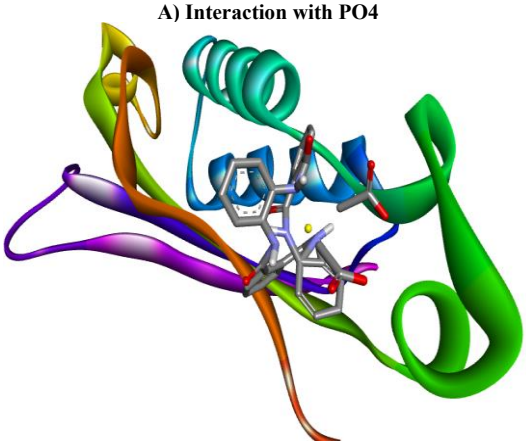

C) Interaction with PO5

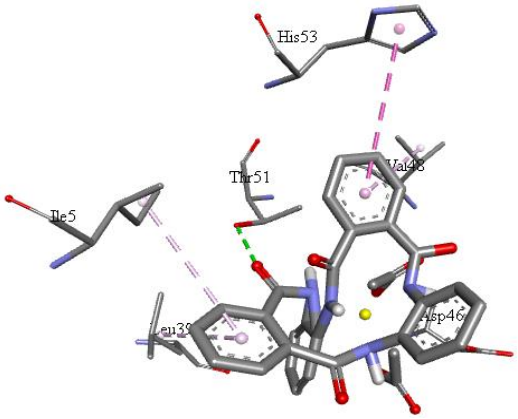

D) 3D Int. with PO5

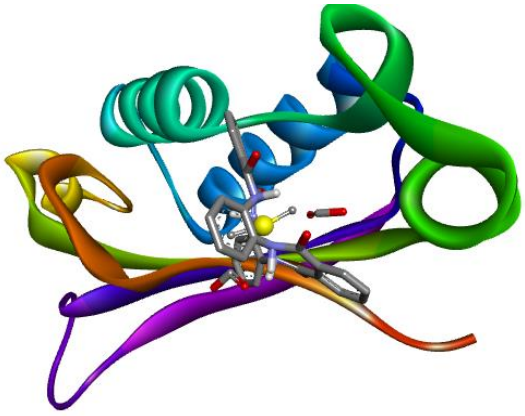

E) Interaction with PO6

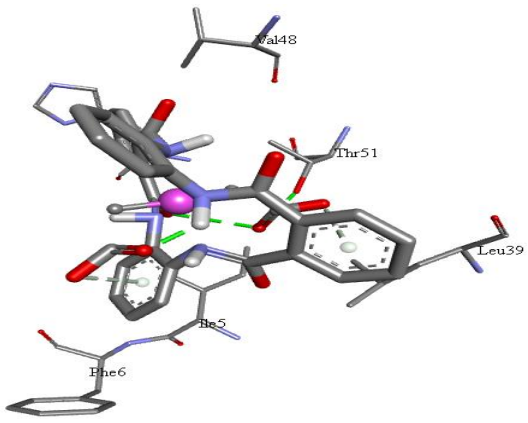

F) 3D interaction with PO6

Fig. 11: Interaction With 2DHN Receptor (Co in Cyan Color, Cu in Pink Color, Ni in Yellow Color).

In contrast, PO7 complex displays the most negative binding energy, 12.4Kcal/mol, with the 3T88 receptor protein with one conventional H-bond interaction. The binding energy for 6IGY, 2W7Q, 5H67, 2DHN, and 3DRA receptor protein observed was -10.0Kcal/mol, -9.8Kcal/mol, -9.8Kcal/mol, -9.6Kcal/mol, and -9.3Kcal/mol with 8, 3, 0, 0, 1 conventional H-bond interactions. PO8 complex exhibited good interaction with all the receptor proteins. The binding energy observed with 2DHN, 5H67, 2W7Q, 3DRA, 3T88 and 6IGY proteins was -9.4Kcal/mol, -10.0Kcal/mol, -10.3Kcal/mol, -10.8Kcal/mol, -13.2Kcal/mol and -12.2Kcal/mol energy. PO9 complex displayed the most negative binding energy -12.7Kcal/mol, with 3DRA and exhibited three H-bond interactions. The binding energy -9.2Kcal/mol, -12.6Kcal/mol, -9.2Kcal/mol, -9.1Kcal/mol and -10.9Kcal/mol were observed with 2DHN, 3T88, 5H67, 2W7Q and 6IGY receptor proteins.

Among the synthesized macrocyclic nitrate complexes, the PO7 complex was found to be strong against *S. aureus,* while PO8 and PO9 were against *A. niger* and *C. albicans,* respectively (Fig. 12 & S13-29).

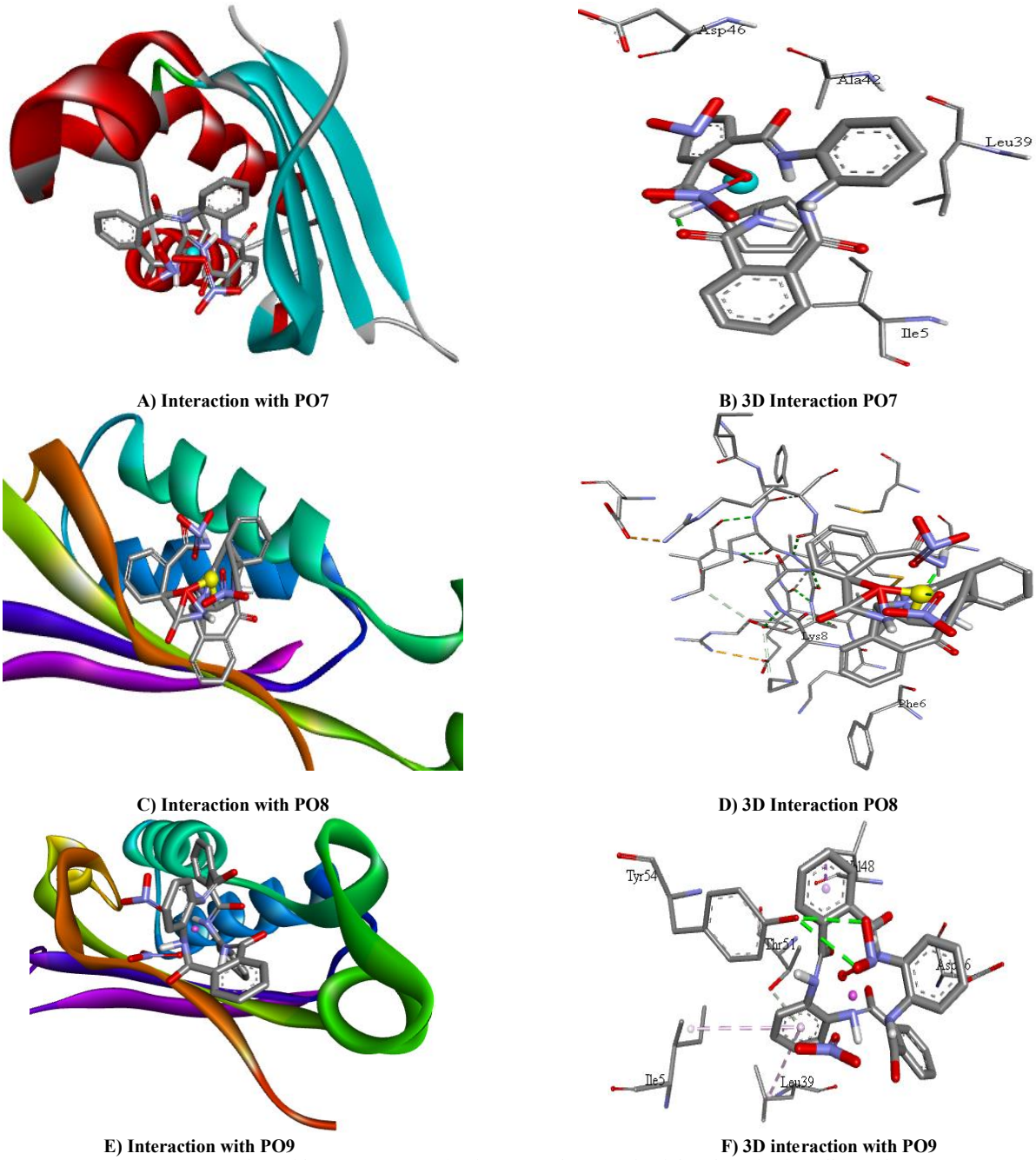

A) Interaction with PO7 **B) 3D Interaction PO7**

C) Interaction with PO8 **D) 3D Interaction PO8**

E) Interaction with PO9 **F) 3D interaction with PO9**

Fig. 12: Interaction With 2DHN Receptor (Co in Cyan Color, Cu Is in Pink Color, Ni Is in Yellow Color).

Table 3: Binding Affinities (Kcal/Mol) of Macrocyclic Metal Chloride Complexes $[M(C_{28}H_{20}N_4O_4)(Cl)_2]$ with Different Protein

Compound	Active Protein (PDB ID)	Binding affinity (Kcal/mol)	No. of H-bonds	Donor atom	Distance (A⁰)
PO1	2DHN	-11.5	1	Val52:O	3.18
	3T88	-12.5	0		
	5H67	-9.5	5	Thr27:O,Ser139:O,Gln143,Cys1114	-
				-	3.09,3.25,2.23,2.82,1.60
	2W7Q	-10.0	3	Gln107:O,Gln42:NE2,Thr44:OG1	2.79,2.80,3.28
	3DRA	-10.7	2	Asn30:ND2,Tyr67:OH	2.88,3.19
	6IGY	-9.8	0	-	-

PO2	2DHN	-9.4	0	-	-
	3T88	-13.8	3	Gln114:NE,Arg64:NH,Asp110:OD1	3.12,3.28,3.32
	5H67	-10.1	1	Ser159:OG	2.36
	2W7Q	-10.7	2	Gln71:NE2, Gln107:O	2.95,3.15
	3DRA	-9.9	2	Lys78:NZ, Lys152:NZ	3.38,3.38
	6IGY	-10.6	3	Tyr111:HN,Tyr150:O,Glu149:O	2.90,3.36,2.82
PO3	2DHN	-8.9	3	Tyr54:OH,Asp46:OD1,Thr51:OG1	3.07,3.03,3.00
	3T88	-12.2	0	-	-
	5H67	-9.6	3	Thr27:O,Cys1114:N,Gln1114:O	3.30,2.30,1.93
	2W7Q	-9.1	2	Thr44:OG1:B,Gln42:NE2	3.19,3.20
	3DRA	-10.2	2	Tyr297:OH,Asp294:OD2	3.28,2.53
	6IGY	-10.9	0	-	-

Table 4: Binding Affinities (Kcal/Mol) of Macrocyclic Metal Acetate Complexes $[M(C_{28}H_{20}N_4O_4)(Ac)_2]$ with Different Proteins

Compound	Active Protein (PDB ID)	Binding affinity (Kcal/mol)	No. of H-bonds	Donor atom	Distance (Aº)
PO4	2DHN	-10.1	2	Asp46,Val52	3.36, 3.52
	3T88	-9.2	0	-	-
	5H67	-8.4	4	Lys145 (2),Glu163,Ser52	2.78,2.60,3.30,2.80
	2W7Q	-9.7	3	Gln77 (2), Gln53	3.07,2.83,3.16
	3DRA	-8.6	1	Glu156	2.99
	6IGY	-9.5	0	-	-
PO5	2DHN	-8.6	1	Thr51	2.70
	3T88	-9.6	0	-	-
	5H67	-9.2	0	-	-
	2W7Q	-9.5	6	Arg104,Gln171,Thr44 (2),Thr173,Gln42	2.83,3.31,2.91,2.80,2.74,3.08
	3DRA	-10.0	3	Ser65,Arg160,Se95	2.41,2.80,1.90
	6IGY	-10.0	0	-	-
PO6	2DHN	-9.2	1	Thr51	2.94
	3T88	-12.9	2	Arg173 (2)	3.07,3.03
	5H67	-10.7	2	Thr27 (2)	2.96,2.80
	2W7Q	-9.8	3	Gln42,Gln171 (2)	2.97,3.30,3.33
	3DRA	-11.3	2	Asn30,Met348	2.62,3.47
	6IGY	-10.4	1	Arg30	2.33

Table 5: Binding Affinities (Kcal/Mol) of Macrocyclic Metal Nitrate Complexes $[M(C_{28}H_{20}N_4O_4)(NO_3)_2]$ with Different Proteins

Compound	Active Protein (PDB ID)	Binding affinity (Kcal/mol)	No. of H-bonds	Donor atom	Distance (Aº)
PO7	2DHN	-9.6	0	-	-
	3T88	-12.4	1	Gln242	3.10
	5H67	-9.8	0	-	-
	2W7Q	-9.8	3	Arg39,Asp72, Lys85	3.72,2.95,2.97
	3DRA	-9.3	1	Asn134	2.31,
	6IGY	-10.0	8	His183,Phe211,Ile188,Asp210 (2),Leu144 (2)	2.45,1.40,2.74,2.03,2.48,2.11,1.85,2.47
PO8	2DHN	-9.4	0	-	-
	3T88	-13.2	3	Cys240,Asp239,Gly242	3.39,3.09,3.42
	5H67	-10.0	1	Thr27	2.35
	2W7Q	-10.3	2	Gln53,Gln171	2.94,2.37
	3DRA	-10.8	2	Lys78,Glu146	2.61,2.43
	6IGY	-12.2	0	-	-
PO9	2DHN	-9.2	2	Tyr54 (2)	2.80,3.11
	3T88	-12.6	1	Gln114	3.26
	5H67	-.9.2	1	Ile141	2.11
	2W7Q	-9.1	3	Gln77,Arg104,Thr44	3.05,2.71,3.31
	3DRA	-12.7	3	Ser95,Tyr67 (2)	3.07,2.22,3.04
	6IGY	-10.9	8	Tyr150 (2),Trp148 (2),Phe115 (2),Val116,Ser113	2.43,3.00,2.89, 2.43,2.23,2.66,2.21,2.63

5. Conclusions

The research presented herein describes the synthesis of nine novel bioactive macrocyclic metal complexes of Co(II), Ni(II), and Cu(II) through a metal ion template condensation approach. The team characterized the complexes by Fourier transform infrared, UV-Visible, mass spectrometry, thermogravimetric (TG) analysis, and EPR studies. Distorted octahedral geometry has been described around the central metal ion of the complexes. Copper macrocyclic complexes possess excellent antimicrobial and antioxidant inhibitory action that may be useful for developing innovative therapeutic drugs for treating a variety of diseases by combining with other antibiotics to enhance their efficacy on bacterial species.

Acknowledgement

The authors are highly grateful to IIT Delhi for providing ESR and TGA analytical facilities. The author is thankful to SAIF-IIT Roorkee for the UV-Visible facility. We are also thankful to G. J. University, Hisar, for Infrared and mass analysis.

Data availability statement

Data supporting the results of this study are available on fair request from the corresponding author.

Funding sources

The author (Indu Sindhu) has received financial support from the Council of Scientific and Industrial Research-University Grants Commission (CSIR-UGC), New Delhi, in the form of a JRF fellowship with reference number 231610039634.

References

[1] Da Silva VS, Teixeira LI, do Nascimento E, Idemori YM, DeFreitas-Silva G, Appl Catal. A: Gen. 2014; 469: 124. https://doi.org/10.1016/j.apcata.2013.09.033.
[2] Da Silva VS, Idemori YM, DeFreitas-Silva G, Appl Catal. A: Gen. 2015; 498: 54. https://doi.org/10.1016/j.apcata.2015.03.022.
[3] Feng Z, Hao F, Liu P, Luo H, J Mol. Catal. A. Chem. 2015; 410: 221. https://doi.org/10.1016/j.molcata.2015.09.027.
[4] Zhou W, Chen D, Sun F, Qian J, He M, Chen Q, Tetrahedron Lett. 2018; 59: 949. https://doi.org/10.1016/j.tetlet.2018.01.094.
[5] Sindhu I, Singh A, Nanotechnology: A boon for the scientific domain, IIP Series, 2024; 3: 1-15. https://doi.org/10.58532/V3BECS22P1CH1.
[6] Singh A, Chaudhary A, Silicon 2019; 11. https://doi.org/10.1007/s12633-018-9971-4.
[7] Nath BD, Takaihi K, Ema T, Catal. Sci. and Technol. 2020; 10: 12. https://doi.org/10.1039/C9CY01894H.
[8] Singh A, Chaudhary A, Bioinorg. Chem. Appl. 2018; 3: 2467463. https://doi.org/10.1155/2018/2467463.
[9] El-Boraey HA, El-Gammal OA, Open Chem. J. 2018; 5: 51. https://doi.org/10.2174/1874842201805010051.
[10] Kumar S, Jha RR, Yadav S, Gupta R, New J. Chem. 2015; 39: 1. https://doi.org/10.1039/C4NJ01300J.
[11] Chaudhary A, Singh A, Int. J. Curr. Res. Med. Sci. 2017; 3: 60-74. https://doi.org/10.22192/ijcrms.2017.03.06.009.
[12] Tazin N, Ragole VD, Wankhede DS, Inorg. Nano-Met. Chem. 2019; 49: 291. https://doi.org/10.1080/24701556.2019.1661449.
[13] Sindhu I, Tomar R, Singh A, Solid base catalysts: Synthesis, characterization and applications, Wiley-VCH GmbH, 2024; 1-25. https://doi.org/10.1002/9783527846719.ch1.
[14] Chaudhary A, Singh A, Int. J. Adv. Res. 2016; 4: 1004-1015. https://doi.org/10.21474/IJAR01/1575.
[15] Singh A, Chaudhary A, J. Iran. Chem. Soc. 2019; 17: 1-11. https://doi.org/10.1007/s13738-019-01829-6.
[16] El-Boraey HA, El-Gammal OA, Spectrochim. Acta A. 2015; 138: 533. https://doi.org/10.1016/j.saa.2014.11.015.
[17] Shalini ASS, Amaladasan M, Prasannbalaji N, Revathi J, Muralithran G, Arabian J. Chem. 2019; 12: 1176. https://doi.org/10.1016/j.arabjc.2014.11.033.
[18] Bansal N, Dave S, Main Group MET. Chem. 2013; 36: 101. https://doi.org/10.1515/mgmc-2012-0074.
[19] Fahmi N, Upadhyay M, Sharma N, Belwal S, J. Chem. Res. 2020; 44: 336. https://doi.org/10.1177/1747519819893885.
[20] Corbin BD, Seeley EH, Raab A, Feldmann J, Miller MR, Torres VJKL, Anderson, Dattilo BM, Dunman PM, Gerads R, Caprioli RM, Nacken W, Chazin WJ, Skaar EP, Sci. 2008; 319: 962. https://doi.org/10.1126/science.1152449.
[21] Baliyan S, Mukherjee R, Priyadarshini A, Vibhuti A, Gupta A, Pandey RP, Chung-Ming Chang, Molecules 2022; 27: 1326. https://doi.org/10.3390/molecules27041326.
[22] Sharma OP, Bhat TK, Food Chem. 2009; 113: 1202. https://doi.org/10.1016/j.foodchem.2008.08.008.
[23] Chaudhary A, Singh A, J. Chem. 2017; 1: 1-19. https://doi.org/10.1155/2017/5936465.
[24] Nozha SG, Morgan SM, Ahmed SEA, El-Mogazy MA, Diab MA, El-Sonbati AZ, Abou-Dobara MI, J. Mol. Struc. 2021; 1127: 129525. https://doi.org/10.1016/j.molstruc.2020.129525.
[25] Mohamed GG, El-Sherif AA, Saad MA, El-Sawy SEA, Morgan SM, J. Mol. Liq. 2016; 223: 1311. https://doi.org/10.1016/j.molliq.2016.09.065.
[26] Trott O, Olson AJ, J. Comput. Chem. 2010; 31: 455. https://doi.org/10.1002/jcc.21334.
[27] Dilip CS, Sivakumar V, Prince JJ, Indian J. Chem. Technol. 2012; 19: 351.
[28] Singh DP, Malik V, Kumar R, Kumar K, Singh J, Russ. J. Coord. Chem. 2009; 35: 740. https://doi.org/10.1134/S1070328409100054.
[29] Katouah H, Hameed AM, Alharbi A, Alkhatib F, Shah R, Chem. Select, 2022; 5: 10256. https://doi.org/10.1002/slct.202002388.
[30] Masih I, Fahmi N, Rajkumar, J. Enzyme Inhib Med. 2013: 28: 33. https://doi.org/10.3109/14756366.2011.625022.
[31] Kamboj M, Jain K, Singh DP, Asian J. Chem. 2018; 30: 1431. https://doi.org/10.14233/ajchem.2018.20984.
[32] Sangwan V, Singh DP, Mater. Sci. Eng. C. 2019; 105: 110119. https://doi.org/10.1016/j.msec.2019.110119.
[33] Kamboj M, Singh DP, Singh AK, Chaturvedi D, J. Mol. Struc. 2020; 1207: 127602. https://doi.org/10.1016/j.molstruc.2019.127602.
[34] Singh DP, Sharma K, Parveen, Asian. J. Chem. 2014; 26: 376. https://doi.org/10.14233/ajchem.2014.15408.
[35] Jasim SA, Riadi Y, Majdi HS, Altimari US, RSC adv. 2022; 12: 17905. https://doi.org/10.1039/D2RA02587F.
[36] Horowitz HH, Metzger G, Anal. Chem. 1963; 35: 1464. https://doi.org/10.1021/ac60203a013.
[37] El-Sonbati AZ, El-Mogazy MA, Nozha SG, Diab MA, Abou-Dobara MI, Eldesoky AM, Morgan SM, J. Mol. Struct. 2022; 1248: 131498. https://doi.org/10.1016/j.molstruc.2021.131498.
[38] Sindhu I, Singh A, Deswal Y, Gupta NM, Chem. & Biodiv. 2024; 22(3): e202402619. https://doi.org/10.1002/cbdv.202402619.
[39] Shakir M, Bano N, Rauf MA, Owais M, J. Chem. Sci. 2017; 129: 1905. https://doi.org/10.1007/s12039-017-1398-8.
[40] Vashistha VK, Kumar A, Russ. J. Inorg. Chem. 2020; 54: 2028. https://doi.org/10.1134/S0036023620140077.
[41] Kumar A, Vashistha VK, Ahmed S, Ali A, Das DK, Anal. Bioanal. Electrochem. 2020; 12: 922.
[42] Ghassemzadeh M, Faghani F, Shirkhani S, Mohsenzadeh F, J. Mol. Struct. 2023; 1295: 136573. https://doi.org/10.1016/j.molstruc.2023.136573.
[43] Nitha LP, Aswathy R, Mathews NE, Kumari BS, Mohanan K, Spectrochim. Acta A 2014; 118: 154. https://doi.org/10.1016/j.saa.2013.08.075.
[44] Beyene BB, Mihirteu AM, Ayana MT, Yibeltal AW, Results Chem. 2020; 2: 100073. https://doi.org/10.1016/j.rechem.2020.100073.
[45] Sindhu I, Singh A, Res. Chem. Intermed. 2024; 50: 413-436. https://doi.org/10.1007/s11164-023-05179-0.
[46] Diab MA, Nozha SG, El-Sonbati AZ, El-Mogazy MA, Morgan SM, Appl. Organomet. Chem. 2019; 33: e5153. https://doi.org/10.1002/aoc.5153.
[47] El-Sonbati AZ, Diab MA, Morgan SM, Abou-Dobara MI, El-Ghettany AA, J. Mol. Struct. 2020; 1200: 127065. https://doi.org/10.1016/j.molstruc.2019.127065.
[48] Sindhu I, Singh A, Deswal Y, Kirar JS, Res. Chem. Intermed. 2025; 51: 839-873. https://doi.org/10.1007/s11164-024-05473-5.
[49] El-Sonbati AZ, Diab MA, Eldesoky AM, Morgan SM, Salem OL, Appl. Organomet. Chem. 2019; 33: e4839. https://doi.org/10.1002/aoc.4839.
[50] Sindhu I, Singh A, Biomet. 2024; 38: 297-320. https://doi.org/10.1007/s10534-024-00655-5.
[51] Bugalia S, Atal K, Dhayal Y, Phageria U, Antican. Pot. Macro Comp. 2025. https://doi.org/10.1021/bk-2025-1492.ch003.
[52] Yadav M, Yadav D, Singh DP, Kapoor JK, Appl. Organomet. Chem. 2025; 39: e7885. https://doi.org/10.1002/aoc.7885.
[53] Sindhu I, Singh A Deswal Y, Gupta NM, Appl. Organomet. Chem. 2025; 39: e70303. https://doi.org/10.1002/aoc.70303.
[54] Khaidir NS, Inrahim SS, Al-Naseeri A, J. Kufa Chem. Sci. 2025; 4: 537-556.